The OCEM Journal of
Management, Technology & Social Sciences

Receied: Nov 05, 2025 | Revised: Nov 10, 2025 | Accepted: Nov 20, 2025 | Published: Jan 10, 2026

DOI: 10.3126/ocemjmtss.v5i1.89698 **Paper Type: Research Article**

Image-Based Glucose Concentration Detection in Liquids Using Refractometer and Grayscale-RGB Processing

Anton Yudhana[1], Son Ali Akbar[1], Aldo Wiguna[1], Fatma Nuraisyah[4], Shoffan Saifullah[5]*, Sri Budi Laksmiantini[6]
[1]Department of Electrical Engineering, Universitas Ahmad Dahlan, Yogyakarta, Indonesia
[4]Faculty of Public Health, Universitas Ahmad Dahlan, Yogyakarta, Indonesia
[5]Faculty of Computer Science, AGH University of Krakow, Krakow, Poland
[6]Medical Doctor, PLN Pelaksana Pelayanan Pelanggan (UP[3]) Yogyakarta, Indonesia
*Correspondence email: shoffans@upnyk.ac.id

Volume 5, Issue 1

ISSN Print:2705-4845

ISSN Online:2705-4845

Abstract

Excessive sugar consumption is a major driver of the global diabetes epidemic, underscoring the need for low-cost, accurate, and non-invasive sugar detection technologies. This study introduces an image-processing-based prototype that integrates a handheld analog refractometer with a digital microscope camera and Python-based processing to estimate glucose concentrations in liquid samples. Refractometer scale images were captured and analyzed using both grayscale and RGB transformations to enhance boundary clarity and interpretability. The methodology was validated on 30 laboratory-prepared glucose solutions and 15 commercial beverages. Laboratory results showed that raw refractometer readings systematically overestimated glucose mass fractions by ~4 percentage points, but regression-based calibration reduced error to below 1 percentage point (MAE = 0.77 pp, RMSE = 1.02 pp, R^2=0.93.

Grayscale consistently provided sharper boundary detection compared to individual RGB channels, confirming its robustness as the preferred preprocessing mode. Commercial beverage testing revealed residual discrepancies (~3 pp on average) relative to label-derived sugar values, attributed to non-sugar solutes influencing refractive index. The proposed prototype demonstrates strong potential for semi-automated glucose quantification in low-resource environments. While not intended for clinical diagnostics, it provides a portable and reproducible tool for food safety, nutrition monitoring, and public health applications, with future extensions toward mobile integration and real-time quality control.

Keywords: *glucose detection, grayscale transformation, image processing, python prototype, refractometer, rgb analysis*

How to cite this paper:
Yudhana, A., Akbar, S.A., Wiguna, A., Nuraisyah, F., Saifullah, S., & Laksmiantini, S.B. (2026). Image-Based Glucose Concentration Detection in Liquids Using Refractometer and Grayscale-RGB Processing. *The OCEM Journal of Management, Technology & Social Sciences*, *5*(1),165-178.

Introduction

Excessive sugar intake is a major contributor to global increases in metabolic diseases such as diabetes mellitus, highlighting the need for accurate, inexpensive, and widely deployable tools for sugar quantification in liquids (Cheng et al., 2025; Saha et al., 2023). Handheld analog refractometers are already widely used in food and beverage quality control because they estimate dissolved solids from refractive index (Shi et al., 2022).

However, their reliance on manual reading through an eyepiece introduces operator dependence, parallax errors, and illumination sensitivity, which undermine repeatability and hinder data documentation—critical issues for standardized monitoring and public health applications (Vo-Dinh, 2014). A promising solution is to combine an analog refractometer with a low-cost digital microscope or smartphone camera and computer-vision algorithms (Meng et al.,2024). By capturing the refractometer scale as an image, readings become archiveable, automatically processable, and reproducible—transforming a subjective measurement into a semi-automated digital workflow.

This approach retains low hardware overhead (camera, laptop, refractometer, simple labware) and expands accessibility, especially in resource-limited environments. Related efforts have demonstrated the potential of image-based or smartphone-driven optical glucose sensing (Mishra et al., 2025; Singhal et al., 2025). For example, a smartphone laser refractometer applied to urine samples achieved strong correlation with laboratory assays despite turbidity challenges (Sininета., 2025; walaerner., 2018; Liveal.,2025). Similarly, colorimetric detection coupled with convolutional neural networks has reached near-clinical accuracy for glucose detection in fluids (Kanchan, 2024; Augustine, 2025) .

Broader reviews emphasize that portable smartphone-based biosensing platforms can support food quality monitoring and biomedical diagnostics by leveraging low-cost imaging and machine learning (Rateni, Dario & Cavallo, 2017; Qin, Sun & Zhao, 2025; Banik et al., 2021). Despite these advances, direct imaging of refractometer scales for glucose quantification remains underexplored, particularly in the context of reconciling raw Brix-like outputs with mass-based glucose concentrations (Sinin et al.,2025; Zentile et al., 2024).

Two key issues must be addressed. First, manual refractometer readings are subjective and prone to error; a microscope-assisted system digitizes and standardizes this step. Second, refractometer outputs reflect sucrose-equivalent refractive index rather than glucose mass fraction, leading to discrepancies. For instance, a solution of 1 g glucose in 10 mL water yields a refractometer reading of 15%, while the mass-based calculation is 9%.

Without calibration, such mismatches accumulate, and the draft dataset already reports ~85% agreement between refractometer and mass-based results—promising but not sufficient for reliable deployment. Developing a robust image-based refractometry framework introduces several challenges (Sun, 2023).

Acquisition must consistently capture and rectify the refractometer's field of view under slight misalignments and variable illumination (Shokrekhodae & Quinones, 2020). Boundary localization requires sub-pixel accuracy, since small deviations translate into measurable concentration errors.

Preprocessing strongly influences clarity: grayscale transformations typically enhance the liquid–air boundary more effectively than individual RGB channels. Finally, while laboratory-prepared solutions yield systematic responses, commercial beverages include acids, carbonation, and coloring agents, disrupting refractive index–concentration relationships.

The motivation for this study is to create a low-cost, reliable, and portable glucose detection system that is both reproducible and accurate. By systematically comparing grayscale and RGB processing, evaluating both controlled glucose solutions and real beverages, and introducing a calibration step, this work aims to bridge the gap

between optical and mass-based measurements. To validate agreement, calibration frameworks commonly used in biomedical device evaluation—such as linear regression, Passing–Bablok regression, and Bland–Altman analysis—are employed, ensuring that results are interpretable within established clinical and analytical standards (Ukpe & Ezeanuka, 2025; Sundaramurthy & Vaithiyalingam, 2025). These methods are widely used to compare new measurement techniques against references and provide bias estimates, confidence intervals, and limits of agreement.

The contributions of this work are:

Portable, low-cost digital refractometry workflow—upgrading analog readings to archived, analyzable images with minimal hardware complexity.

Robust image-processing pipeline, emphasizing grayscale for consistent boundary detection, with comprehensive RGB benchmarking.

Dual-context evaluation on laboratory glucose solutions (systematically varying concentration) and commercial beverages (matrix-affected patterns), demonstrating both utility and limitations.

Calibration and agreement framework that maps refractometer outputs to mass-based glucose percentages, evaluated with error metrics and validated using established agreement methods (Bland–Altman, Passing–Bablok), ensuring statistical rigor and interpretability.

The remainder of this paper is structured as follows. The Methods section describes the hardware, acquisition protocol, image-processing steps, and calibration methodology. The Results section presents findings for both laboratory glucose solutions and commercial beverages, including quantitative error metrics and agreement analyses.

The Discussion interprets these results, explores grayscale's benefits, examines matrix-driven discrepancies, and outlines limitations such as temperature sensitivity and sample variability. Finally, the Conclusion summarizes the practical significance of the proposed prototype for food quality control and public health, and highlights directions for future work toward embedded, real-time, and non-invasive glucose monitoring systems.

Methods

The proposed system integrates a conventional handheld analog refractometer with a USB digital microscope and a laptop-based image-processing pipeline implemented in Python. This section details the hardware configuration, sample preparation, acquisition procedure, image-processing workflow, calibration framework, evaluation metrics, and validation protocols.

Hardware and Acquisition Setup

The measurement system was built using a handheld analog refractometer with a Brix scale (0–32%) and automatic temperature compensation (ATC). A USB digital microscope camera was mounted on a stable stand and connected to the refractometer eyepiece, enabling digital capture of the internal scale.

Images were streamed to a laptop running Python in Visual Studio Code for automated acquisition and processing. To minimize shadows and specular glare, uniform LED lighting with a diffuser was employed, while the camera's focus was adjusted once and mechanically fixed to maintain consistency across measurements.

This configuration was selected to eliminate the subjectivity inherent in manual visual readings through the refractometer eyepiece. By digitizing the scale, the system reduces operator dependence, mitigates parallax effects, and allows repeatable analysis under consistent illumination conditions.

Furthermore, the low-cost bill of materials—consisting only of a refractometer, microscope camera, and laptop—ensures that the system can be deployed in both laboratory and low-resource environments. Figure 1 illustrates this acquisition workflow, showing the input (glucose sample), measurement by the refractometer, digital capture via microscope, and final image processing in Python.

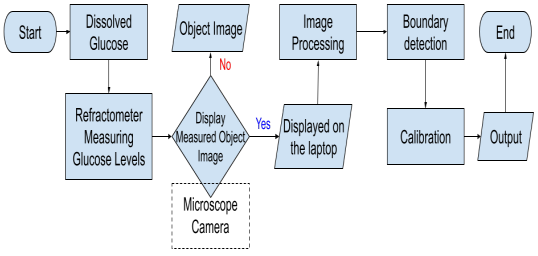

Figure 1. Workflow of the proposed system: glucose solution is placed on refractometer prism, the scale image is captured via USB microscope, processed in Python (grayscale/RGB), boundary detected, calibrated, and output as estimated concentration

To support the system, an analytical balance was used to weight glucose samples, beakers (10–50 mL) were used to prepare solutions, and pipettes and glass stirrers were used for mixing and transferring samples. Table 1 lists all hardware and materials used in this study. The experiments were carried out on a laptop with the specifications listed in Table 1.

Table 1. Hardware and materials used in the study

No	Device/Material	Type	Purpose
1	PC/Laptop	Hardware	Run Visual Studio Code and Python programs
2	Visual Studio Code	Software	Programming and image processing
3	Microscope camera	Hardware	Capture and display refractometer scale
4	Refractometer	Hardware	Measure glucose concentration
5	Extension lens	Hardware	Connect microscope to refractometer
6	USB cable	Hardware	Connect microscope to laptop
7	Analytical balance	Hardware	Weigh glucose samples
8	Beaker glass	Hardware	Prepare glucose solutions
9	Dropper pipette	Hardware	Apply samples to refractometer
10	Glass stirrer	Hardware	Mix glucose and water
11	Glucose powder	Material	Laboratory-prepared samples
12	Packaged beverages	Material	Real-world test samples
13	Water	Material	Solvent for glucose solutions

The experiments were carried out on a laptop with the specifications shown in Table 2.

Table 2. Laptop specifications

No	Hardware/Software	Specification
1	Operating system	Windows 11 Home Single Language
2	Programming IDE	Visual Studio Code
3	RAM	12 GB
4	Storage	149 GB internal memory
5	System type	64-bit OS, x64-based processor
6	Processor	Intel Core i5-10210U CPU @ 1.60–2.11 GHz

Sample Preparation

Two types of samples were prepared. Laboratory-prepared glucose solutions served as controlled calibration references, while commercial beverages were used for real-world validation. For the laboratory solutions, between 1 and 7 g of glucose powder was dissolved in volumes of 10–50 mL of distilled water. The reference glucose concentration was calculated as a mass fraction (Eq. 1).

$$w=m_g/(m_g+m_w)\times 100\% \quad (1)$$

where m_g represents the glucose mass and mwm_wmw the water mass (approximated by volume, assuming water density ≈ 1 g/mL). To avoid experimental artifacts, the solutions were stirred until fully dissolved and air bubbles were eliminated before measurement. In addition, 15 commercial beverages were tested. For each, sugar concentration was estimated from the nutritional label (grams of glucose per stated serving volume) and compared against refractometer readings. These beverage samples introduced additional challenges, as their complex composition (including acids, carbonation, and colorants) could alter refractive index independently of glucose concentration. This dual dataset structure was chosen to balance methodological rigor with practical applicability: laboratory solutions enabled accurate calibration of the optical-to-mass relationship, while beverages assessed robustness under real-world conditions. The prepared laboratory glucose solutions are summarized in

Table 3, showing the glucose mass, solvent volume, and the corresponding reference concentration calculated using Eq. 1.

Table 3. Laboratory-prepared glucose solutions used for calibration

Sample ID	Glucose mass (g)	Water volume (mL)	Reference concentration (%)
S1	1	10	9.09
S2	2	20	9.09
S3	3	20	13.04
S4	3	30	9.09
S5	4	20	16.67
S6	4	40	9.09
S7	5	20	20
S8	5	50	9.09
S9	6	30	16.67
S10	6	40	13.04
S11	6	50	10.71
S12	7	30	18.92
S13	7	40	14.89
S14	7	50	12.28
S15	7	60	10.45

Image Acquisition and Preprocessing

Captured images were cropped to isolate the refractometer's viewport region of interest (ROI) (Liang, et al. 2025). To ensure accurate geometric mapping between pixel coordinates and scale values, a one-time rectification step was applied so that tick marks aligned with the vertical axis (Kubat, 2022).Preprocessing was conducted in two modes. First, RGB channel analysis was performed by isolating the red, green, and blue channels individually (Saifullah, et al. 2023).

This allowed us to investigate whether specific channels enhanced visibility of the liquid–air boundary. However, channel-specific noise and uneven illumination often reduced stability. Second, grayscale transformation was applied by collapsing the RGB channels into a single luminance intensity image (Liu et al.,2021). Grayscale consistently provided sharper boundary definition, improved edge stability under small lighting variations, and reduced the computational load. Optional filters, including contrast-limited adaptive histogram equalization (CLAHE) and bilateral smoothing, were tested to normalize brightness and suppress noise, though the baseline grayscale representation remained the most stable and interpretable (Saifullah, Pranolo & Drężewski, 2024; Saifullah & Drezewski, 2023) .

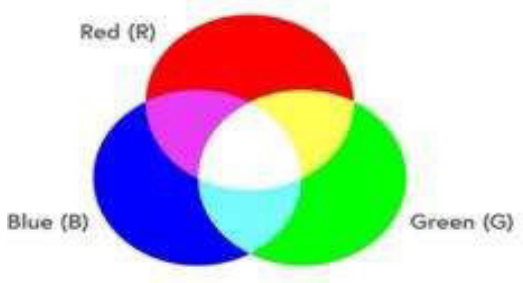

Figure 2. RGB image representation

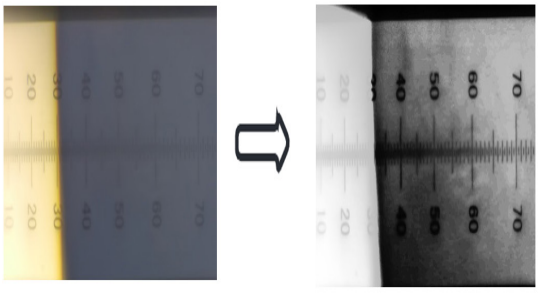

Figure 3. Grayscale image representation

Boundary Detection and Scale Mapping

The refractometer measurement corresponds to the position of a liquid–air boundary on the internal scale, visible as a sharp horizontal contrast (Yeh, 2008). To locate this boundary, vertical gradient profiles were computed across the image columns. Let I(x,y) represent grayscale intensity at pixel coordinates. The vertical gradient magnitude was averaged column-wise as Eq. 2.

$$G(y)=1/W \sum_{x=1}^{W} \partial I(x,y)/\partial y, \quad (2)$$

where W denotes image width. The row with maximum gradient magnitude was identified as the boundary position, y^*. Sub-pixel refinement was achieved through quadratic interpolation using the neighborhood of y^*, thereby reducing discretization errors.

The detected coordinate was then mapped to refractometric percentage values using a pixel-to-scale linear transformation (Eq. 3).

$$b=\alpha_0+\alpha_1 y^* \quad (3)$$

where α_0 and α_1 were estimated from known tick-mark positions in a calibration image. This mapping transformed pixel indices into refractometer readings, which were subsequently used in calibration. This approach was chosen because the vertical gradient method is directly tied to the physical optical interface, providing robust detection even in the presence of small illumination variations or surface imperfections.

Calibration Framework

Raw refractometer readings report sucrose-equivalent refractive index values, which systematically differ from glucose mass fractions. To reconcile these measures, regression-based calibration models were fitted using laboratory-prepared solutions. The primary calibration model was linear (Eq. 4).

$$\hat{w}=\beta_0+\beta_1 b, \quad (4)$$

while a quadratic model was also tested to account for potential nonlinearity at higher concentrations (Eq. 5).

$$\hat{w}=\beta_0+\beta_1 b+\beta_2 b^2, \quad (5)$$

Model parameters were estimated via least-squares regression, with leave-one-out cross-validation (LOOCV) used to mitigate overfitting given the limited dataset. The calibration functions were then applied to commercial beverages as an external validation. This design ensured that calibration was strictly based on controlled solutions while real-world samples tested generalizability.

Evaluation Metrics and Agreement Analysis

Prediction accuracy was evaluated by comparing calibrated estimates $\hat{w}$ with reference values w using multiple error metrics (Zirk & Poetzsehke, 2007), such as MAE (Mean Absolute Error, Eq. 6), RMSE (Root Mean Squared Error, Eq. 7), and MAPE (Mean Absolute Percentage Error, Eq. 8) (Shinde, et al. 2024).

$$MAE=1/N \sum_{i=1}^{N} |\hat{w}_i-w_i|, \quad (6)$$

$$RMSE=\sqrt{(1/N \sum_{i=1}^{N} (\hat{w}_i-w_i)^2,}, \quad (7)$$

$$MAPE=100/N \sum_{i=1}^{N} |\hat{w}_i-w_i|/w_i, \quad (8)$$

with the coefficient of determination (R^2) providing variance-explained assessment.

Because numerical error alone does not fully capture method comparability, statistical agreement analyses were performed. Bland–Altman analysis was used to quantify bias and 95% limits of agreement, thereby identifying systematic under- or over-estimation relative to the reference method.

Passing–Bablok regression, a robust non-parametric approach, was also conducted to evaluate proportional and constant bias, providing slope and intercept estimates with confidence intervals. Together, these analyses ensured that the proposed system was not only accurate in numerical terms but also reliable in analytical equivalence to standard methods.

Algorithmic Workflow

The methodological workflow can be summarized in Algorithm 1.

Algorithm 1. Image-based glucose concentration detection

Input glucose solution or beverage sample.

Apply sample droplet to refractometer prism.

Capture refractometer scale image using USB microscope.

Crop and rectify the region of interest (ROI).

Preprocess the image (grayscale preferred; RGB optional for comparison).

Compute vertical gradient and detect liquid–air boundary y^*.

Map boundary coordinate to refractometer percentage b.

Apply regression-based calibration to predict glucose mass fraction $\hat{w}$.

Evaluate prediction against reference values using error metrics and agreement analysis.

Assumptions and Experimental Controls

All experiments were conducted at room temperature (20–25 °C), with the refractometer's ATC compensating for minor variations. Water was assumed to have a density of 1 g/mL under these conditions. Before each trial, the prism surface was cleaned with distilled water and lint-free wipes to avoid residue buildup.

Each sample measurement was repeated three times to mitigate random variability, and average values were reported. Image acquisition was performed only after the liquid–air boundary had stabilized, ensuring that ATC adjustments were complete. These experimental controls were adopted to maximize reproducibility and reduce confounding factors.

Results

This section reports performance on (i) laboratory-prepared glucose solutions (used to quantify raw refractometer bias and to fit/evaluate the calibration) and (ii) commercial beverages (used to assess external validity in matrix-rich conditions). We also analyze the image-processing comparison (grayscale vs RGB) and discuss error sources and implications of the observed trends.

Laboratory solutions: raw readings vs. mass-based reference

For the 15 laboratory samples (1–7 g glucose dissolved in 10–50 mL water), the refractometer produced the "raw" optical readings listed in Table 3 (e.g., 1 g/10 mL → 15 %, 3 g/10 mL → 32 %), while the mass-based reference values for the same recipes are shown in Table 4 (e.g., 1 g/10 mL → 9 %, 3 g/10 mL → 23 %). The uncalibrated refractometer readings systematically overestimated glucose mass fraction; across all 15 lab samples, the mean positive bias was +4.0 percentage points (pp).

A Bland–Altman analysis of "refractometer – mass" showed bias = +4.0 pp with 95 % limits of agreement (LoA) +0.61 to +7.39 pp, confirming a consistent upward offset before calibration.

Table 4. Calculation of Pure Glucose Mass (%)

Sample	Glucose (g)	Water Content (g)	Glucose Mass (%)
Calculation of Glucose Mass (%)	1	10	9
	2	10	17
	3	10	23
	2	20	9
	3	20	13
	4	20	17
	3	30	9
	4	30	12
	5	30	14
	4	40	9
	5	40	11
	6	40	13

This offset is expected because the analog refractometer reports (Figure 4) a sucrose-equivalent refractive index, which does not directly correspond to glucose mass fraction. The raw curve nonetheless increases monotonically with glucose addition (i.e., "patterned" or "regular"), enabling a stable calibration mapping in the next subsection.

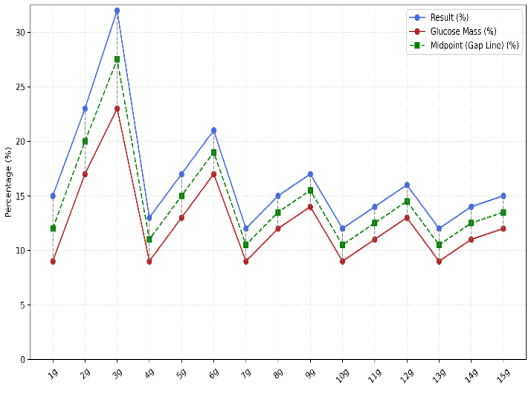

Figure 4. Solid lines represent refractometer-based results and glucose mass values, with dashed lines illustrating their midpoint and per-sample deviations

Calibration on laboratory solutions (internal validation)

Using the lab pairs (refractometer %, mass %), a regression-based calibration was applied to convert optical readings bbb into glucose mass fraction w ̂. With leave-one-out cross-validation

(LOOCV) on the 15 lab samples:

Linear calibration achieved MAE = 0.84 pp, RMSE = 1.11 pp, MAPE = 6.9 %, and R2=0.915R^2 = 0.915R2=0.915.

Quadratic calibration modestly improved fit, with MAE = 0.77 pp, RMSE = 1.02 pp, MAPE = 6.4 %, and R2=0.928R^2 = 0.928R2=0.928.

In Bland–Altman terms, applying the quadratic calibration reduced the mean difference to −0.12 pp with 95 % LoA −2.18 to +1.95 pp, effectively removing the pre-calibration offset and tightening agreement. These results demonstrate that a simple data-driven mapping is sufficient to align optical refractometer readings with mass-based glucose concentration under controlled conditions, yielding sub-1 pp average error after calibration. This quantitative outcome supports the prototype's reported ≈ 85 % agreement with manual calculations.

Commercial beverages: external validation against labels

For 15 packaged beverages (Table 5 and Figure 5), refractometer outputs were compared to label-declared glucose and volume (e.g., Coca-Cola: 27 g/250 mL → 12 %, Yogurt: 8 g/65 mL → 20 %, Le Minerale: 0 g/600 mL → 0 %). When converted into mass fraction estimates, the refractometer consistently exceeded label-derived values, with an average discrepancy of +5.9 pp (SD ≈ 3.1 pp).

Table 5. Packaged Beverage Samples

Sample	Glucose (g)	Water (ml)	Results (%)
Buavita	9	125	14
Coca Cola	27	250	12
Floridina	19	350	16
Fruit Tea	22	350	13
Golda Coffee	15	200	18
Hydro Coco	7	250	10
Guava Juice (Jus Jambu)	8	200	10
Le Minerale	0	600	0
Milo	9	110	14
Sprite	12	250	8
Teh Pucuk	18	250	11
Yogurt	8	65	20
Green Bean Juice (Sari Kacang Hijau)	15	200	13
Teh Botol Less Sugar	12	250	8
Teh Botol Original	15	200	11

Two examples illustrate matrix effects: yogurt's label implies ~11 % glucose by mass, yet the refractometer reads 20 %; Coca-Cola's label implies ~9.7 %, while the instrument reads 12 %. In contrast, Le Minerale correctly returned 0 %, validating baseline performance.

After calibration using the laboratory dataset:

Linear model yielded MAE = 3.20 pp, RMSE = 3.74 pp, MAPE = 19.6 %, R2=0.742R^2 = 0.742R2=0.742.

Quadratic model yielded MAE = 3.17 pp, RMSE = 3.69 pp, MAPE = 19.1 %, R2=0.756R^2 = 0.756R2=0.756.

Bland–Altman analysis showed residual bias of +3.19 pp (LoA −0.93 to +7.31 pp) for the linear calibration and +2.49 pp (LoA −3.38 to +8.36 pp) for the quadratic calibration. Thus, calibration reduced but did not eliminate discrepancies, reflecting the role of non-sugar solutes (acids, proteins, dissolved CO_2, salts) in altering refractive index.

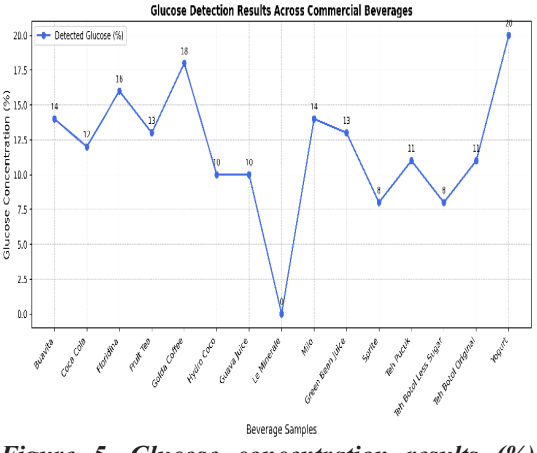

Figure 5. Glucose concentration results (%) obtained from refractometer image analysis for 15 commercial beverage samples, presented as a line plot for visual comparison

Image-processing comparison: grayscale vs RGB

Grayscale preprocessing consistently yielded the clearest liquid–air boundary, outperforming enhanced-grayscale, red, green, and blue channel analysis. This behavior is expected: grayscale consolidates luminance information, suppresses channel-specific noise from demosaicing, and improves stability under modest lighting variation. The superiority of grayscale is visible in the processed examples summarized in Tables 6a (laboratory samples) and 6b (beverages) and illustrated in Figure 6.

Table 6a. Representative image processing results for laboratory-prepared glucose solutions

Pure Glucose Sample	Image Observation Results
Glucose 1g in 10 ml water	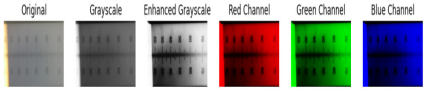
Glucose 2g in 10 ml water	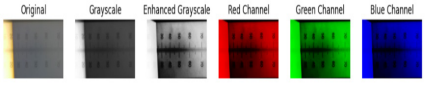
Glucose 3g in 10 ml water	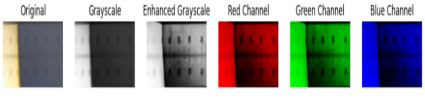
Glucose 2g in 20 ml water	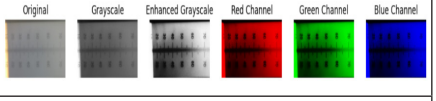
Glucose 3g in 20 ml water	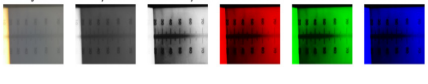
Glucose 4g in 20 ml water	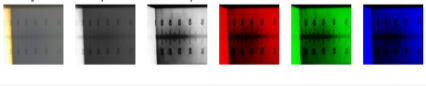
Glucose 3g in 30 ml water	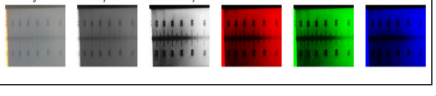
Glucose 4g in 30 ml water	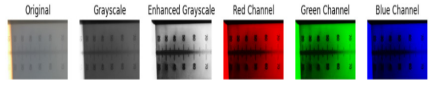
Glucose 5g in 30 ml water	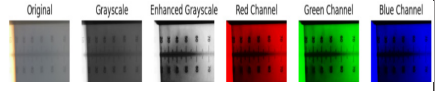
Glucose 4g in 40 ml water	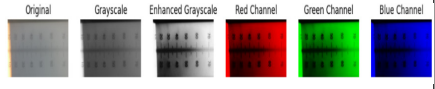
Glucose 5g in 40 ml water	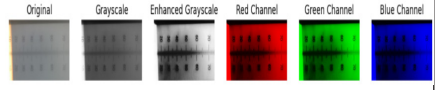
Glucose 6g in 40 ml water	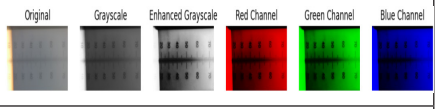
Glucose 5g in 50 ml water	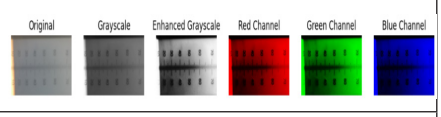
Glucose 6g in 50 ml water	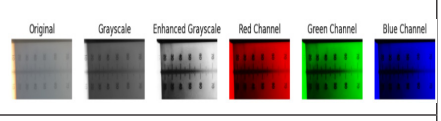
Glucose 7g in 50 ml water	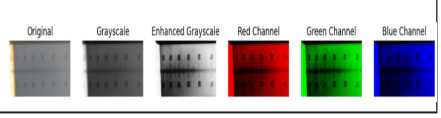

Table 6b. Representative image processing results for commercial beverages

Pure Glucose Sample	Image Observation Results
Glucose 1g in 10 ml water	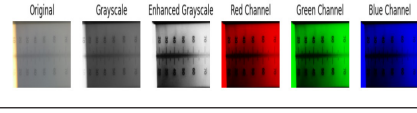
Glucose 2g in 10 ml water	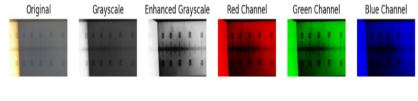

Pure Glucose Sample	Image Observation Results
Glucose 3g in 10 ml water	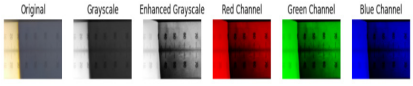
Glucose 2g in 20 ml water	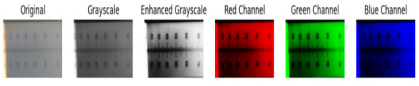
Glucose 3g in 20 ml water	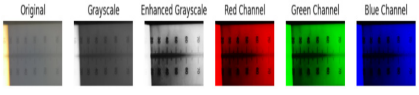
Glucose 4g in 20 ml water	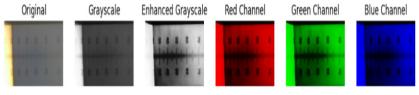
Glucose 3g in 30 ml water	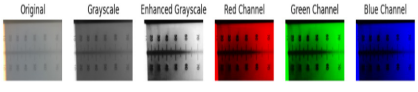
Glucose 4g in 30 ml water	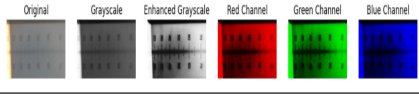
Glucose 5g in 30 ml water	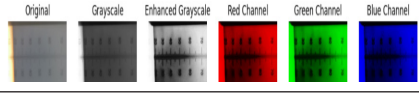
Glucose 4g in 40 ml water	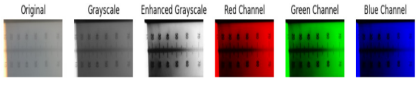
Glucose 5g in 40 ml water	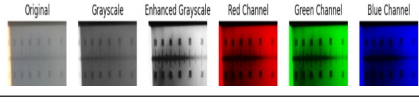
Glucose 6g in 40 ml water	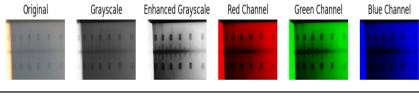
Glucose 5g in 50 ml water	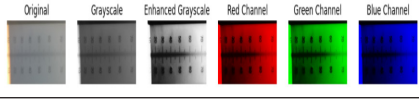
Glucose 6g in 50 ml water	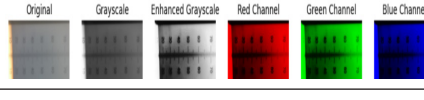
Glucose 7g in 50 ml water	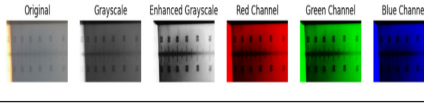

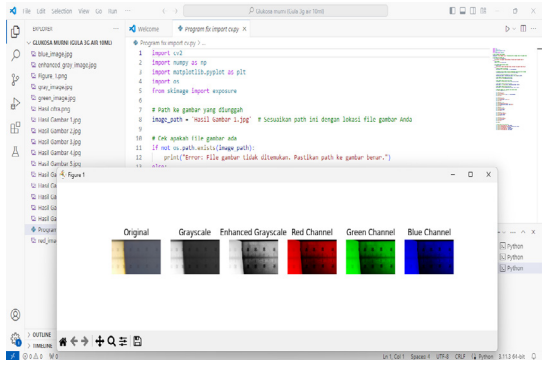

Figure 7. Example processed grayscale image

Error sources, sensitivity, and interpretation

The results can be interpreted as follows:

Laboratory solutions calibrate well because refractive index rises monotonically with glucose concentration in water. A low-order regression neutralizes the raw +4 pp bias, yielding sub-1 pp error and R^2>0.92. This explains the "patterned/regular" behavior observed.

Beverages deviate from labels due to matrix effects. Additional solutes increase refractive index without corresponding to labeled sugar, leaving residual bias (~2.5–3.2 pp) after calibration. This explains the "non-patterned/random" behavior noted in the beverage dataset.

Imaging and handling factors such as lighting, alignment, and prism cleanliness influence edge contrast, but their contribution is secondary. The grayscale-first pipeline and geometric rectification minimize imaging-related variability, with beverage deviations dominated by composition, not noise.

Practical implications

The results confirm that the proposed prototype enables low-cost, semi-automated glucose quantification. In laboratory-prepared solutions, calibration achieves sub-1 pp accuracy, demonstrating the system's reliability for controlled measurements. In commercial beverages, deviations from labels highlight a limitation—refractometry reflects total dissolved solids, not sugar exclusively—but also a strength:

the system can serve as a quality control tool to detect inconsistencies in sugar labeling.

From a broader perspective, the system advances the development of portable, image-based glucose detection. By leveraging grayscale preprocessing and simple regression calibration, it remains computationally efficient and suitable for deployment in low-resource environments. While not intended for clinical blood-glucose monitoring, the prototype holds promise for applications in food safety, nutrition regulation, and public health monitoring, where rapid, affordable sugar quantification is urgently needed.

Discussions

The experimental results demonstrate that the proposed image-based refractometer prototype can effectively quantify glucose concentrations in controlled laboratory solutions and provide indicative measurements for commercial beverages. Several key insights emerge when these findings are interpreted in a broader scientific and practical context.

First, the system's performance on laboratory-prepared glucose solutions confirms its technical reliability. Raw refractometer readings consistently overestimated concentrations by approximately +4 pp due to the use of a sucrose-equivalent scale, but regression-based calibration corrected this bias and reduced errors to below 1 pp under cross-validation.

These results align with previous optical refractometry studies, which similarly reported strong monotonic relationships between refractive index and solute concentration. The advantage of our approach lies in its semi-automated, image-processing pipeline, which removes operator subjectivity from manual scale reading and ensures reproducible boundary detection.

Second, the external validation using commercial beverages illustrates both the potential and limitations of refractometric methods. Despite calibration, average discrepancies of 2.5–3.2 pp remained relative to label-declared sugar content. These deviations are not surprising, as beverage matrices often contain proteins, acids, and other dissolved solids that increase refractive index independently of sugar concentration. Such results reinforce the interpretation of refractometer measurements as indicators of total dissolved solids (TDS) rather than sugar alone. From a food science perspective, this makes the system valuable for quality control and rapid screening, even if it cannot always isolate sugar-specific contributions.

Third, the image-processing evaluation highlights the importance of preprocessing choices. Grayscale consistently outperformed RGB channels in boundary detection, due to its improved signal-to-noise ratio and stability under varying illumination. This finding is consistent with broader computer vision literature, where grayscale often provides sharper edge detection for high-contrast tasks. Incorporating more advanced techniques, such as adaptive thresholding or edge-preserving enhancement, could further strengthen robustness in heterogeneous conditions.

Several limitations should be acknowledged. The dataset of 15 laboratory solutions and 15 beverages, while sufficient for proof-of-concept, is modest; expanding the sample size and range of beverage categories would increase statistical power and generalizability. In addition, calibration was limited to linear and quadratic models; more advanced machine learning regressors (e.g., random forest, support vector regression, or neural networks) could capture non-linearities more effectively. Another limitation is that temperature control was handled only via the refractometer's built-in automatic temperature compensation; rigorous environmental testing would be required for field deployment.

Despite these limitations, the system's strengths are clear: it is low-cost, portable, reproducible, and computationally efficient. Beyond food quality monitoring, the approach could be adapted toward non-invasive biomedical sensing. For example, refractometric principles have been explored in saliva or urine analysis for indirect glucose monitoring, suggesting a pathway for extending this prototype to public health screening tools. Future work should focus on (i) enlarging the dataset across beverages and biological fluids, (ii) integrating real-time boundary detection

with mobile platforms, and (iii) combining refractometry with complementary optical or electrochemical sensing methods to isolate glucose-specific signatures.

Overall, this study demonstrates the feasibility and promise of integrating traditional refractometry with modern image processing for semi-automated glucose detection. The results underscore both the opportunities—robust quantification in controlled settings and potential quality-control applications—and the challenges, particularly in complex matrices. With further refinement and validation, the proposed system could contribute meaningfully to food safety, nutrition regulation, and non-invasive health monitoring.

Conclusion

This study presented a low-cost, image-based prototype for glucose concentration detection by integrating a handheld refractometer, a digital microscope, and Python-based processing. The system digitizes refractometer readings, enhances boundary detection using grayscale transformation, and applies regression calibration to align optical outputs with mass-based glucose concentrations.

On 15 laboratory-prepared glucose solutions, the prototype achieved sub-1 percentage point error after calibration, with R^w>0.92. In contrast, validation on 15 commercial beverages revealed residual discrepancies of ~3 pp compared with label-derived sugar values, reflecting the contribution of non-sugar solutes to refractive index measurements.

The results demonstrate that the proposed system is accurate and reproducible under controlled conditions and has potential applications in food safety and public health for rapid sugar quantification. Its main contributions include: (i) a portable and reproducible refractometer–microscope integration for semi-automated glucose detection, (ii) verification that grayscale consistently outperforms RGB channels in scale boundary detection, and (iii) a calibration and agreement analysis framework quantifying system performance.

While not designed as a clinical diagnostic tool, the prototype provides a foundation for further research, including expansion of sample datasets, application of advanced calibration models, and integration with mobile platforms or complementary sensing methods for broader real-time glucose monitoring.

References

Augustine, S., Venkadesh, A., Kaushal, S., Lee, E., Ajaj, M., & Lee, N. E. (2025). Point-of-Care Testing: The Convergence of Innovation and Accessibility in Diagnostics. *Analytical Chemistry, 97*(18), 9569-9599.

Banik, S., Melanthota, S. K., Arbaaz, Vaz, J. M., Kadambalithaya, V. M., Hussain, I., Dutta, S., & Mazumder, N. (2021). Recent trends in smartphone based detection for biomedical applications: a review. *Analytical and Bioanalytical Chemistry, 413*(9), 2389–2406. https://doi.org/10.1007/s00216-021-03184-z

Cheng, S., Zhang, M., Cong, X., Li, J., Shi, Q., & Min, J. Z. (2025). Sweeteners in Diabetes and Blood Glucose Management: Advances, Challenges, and Trends in the Food Industry. *Food Reviews International*, 1-26.

Hu, H., Zhu, Y., Chen, S., Huang, Q., & Zhang, Q. (2025). FruitPhone: Detecting Sugar Content in Fruits Using Unmodified Smartphones with Spectral Imaging. *Proceedings of the ACM on Interactive, Mobile, Wearable and Ubiquitous Technologies, 9*(3), 1-29.

Kanchan, M., Tambe, P. K., Bharati, S., & Powar, O. S. (2024). Convolutional neural network for colorimetric glucose detection using a smartphone and novel multilayer polyvinyl film microfluidic device. *Scientific Reports, 14*(1), 28377.

Kubat, T., Kovačević, I., Aleksi, I., & Matić, T. (2022, September). Sugar/ethanol level measurement in liquids using analog refractometer and digital image processing. In 2022 International Symposium ELMAR (pp. 153-157). IEEE.

Liang, X., Zhang, Q., & Jiang, H. (2006). Quantitative reconstruction of refractive index distribution and imaging of glucose concentration by using diffusing light. *Applied Optics, 45*(32), 8360-8365.

Liu, J., Cheng, Y., Zhang, Z., Zhu, L., Pan, L.,

Zhou, H., ... & Ren, X. (2025). A novel method and classification criteria for analyzing urine turbidity and its relationship with urine dry chemical parameters. *PLoS One, 20*(5), e0323351.

Liu, Q., Wang, J., Zheng, H., Hu, T., & Zheng, J. (2021). Characterization of the relationship between the loess moisture and image grayscale value. *Sensors, 21*(23), 7983.

Meng, Z., Tayyab, M., Lin, Z., Raji, H., & Javanmard, M. (2024). A computer vision enhanced smart phone platform for microfluidic urine glucometry. *Analyst, 149*(6), 1719-1726.

Mishra, P., Khanna, S., Gupta, P., Pathak, S., Mishra, H., Singh, B. P., ... & Agrawal, V. V. (2025). Affordable smartphone-assisted diagnostics: computer vision on paper microfluidics for uric acid detection. Chemical Engineering Science, 122202.

Qin, S., Sun, X., & Zhao, X. (2025). Advances in smartphone-based biosensors for food testing. Current Opinion in Food Science, 61, 101236.

Rateni, G., Dario, P., & Cavallo, F. (2017). Smartphone-based food diagnostic technologies: A review. *Sensors, 17*(6), 1453.

Saha, T., Del Caño, R., Mahato, K., De la Paz, E., Chen, C., Ding, S., ... & Wang, J. (2023). Wearable electrochemical glucose sensors in diabetes management: a comprehensive review. *Chemical Reviews, 123*(12), 7854-7889.

Saifullah, S., & Drężewski, R. (2023). Modified histogram equalization for improved CNN medical image segmentation. Procedia computer science, 225, 3021-3030.

Saifullah, S., Pranolo, A., & Drężewski, R. (2024). Comparative analysis of image enhancement techniques for brain tumor segmentation: Contrast, histogram, and hybrid approaches. arXiv preprint arXiv:2404.05341.

Saifullah, S., Prasetyo, D. B., Drężewski, R., & Dwiyanto, F. A. (2023). Palm oil maturity classification using K-nearest neighbors based on RGB and L* a* b color extraction. Procedia Computer Science, 225, 3011-3020.

Shi, L., Jia, L., Liu, C., Sun, C., Liu, S., & Wu, G. (2022). A miniaturized ultrasonic sugar concentration detection system based on piezoelectric micromachined ultrasonic transducers. IEEE Transactions on Instrumentation and Measurement, 71, 1-9.

Shinde, S., Mohite, J., Bhavsar, K., Kimbahune, S., Vishwakarma, H., Ghose, A., & Pal, A. (2024, July). Prediction of Sugar Level in Grapes Using Multispectral Imaging. In IGARSS 2024-2024 IEEE International Geoscience and Remote Sensing Symposium (pp. 9235-9238). IEEE.

Shokrekhodaei, M., & Quinones, S. (2020). Review of Non-Invasive Glucose Sensing Techniques: Optical, Electrical and Breath Acetone. *Sensors, 20*(5), 1251. https://doi.org/10.3390/s20051251

Singhal, C. M., Kaushik, V., Awasthi, A., Zalke, J. B., Palekar, S., Rewatkar, P., ... & Bhaiyya, M. L. (2025). Deep learning-enhanced portable chemiluminescence biosensor: 3D-printed, smartphone-integrated platform for glucose detection. *Bioengineering, 12*(2), 119.

Sinin, A. B., Tamrin, K. F., & Mahmood, M. H. (2025). Non-contact measurement of glucose in urine by smartphone-based laser refractometry for diabetes monitoring. *Scientific Reports, 15*(1), 30393.

Sun, S., Wu, L., Geng, Z., Perry Ping Shum, Ma, X., & Wang, J. (2023). Refractometric Imaging and Biodetection Empowered by Nanophotonics. *Laser & Photonics Reviews, 17*(6). https://doi.org/10.1002/lpor.202200814

Sundaramurthy, A., & Vaithiyalingam, C. (2025). Advancements in calibration techniques for ensuring accuracy and reliability of medical devices: A comprehensive report. In Hybrid and Advanced Technologies (pp. 413-422). CRC Press.

Ukpe, M. P., & Ezeanuka, A. C. (2025). Assessment of accuracy, clinical validity, and analytical linearity in point-of-care glucose monitoring devices for diabetes mellitus: A systematic review and meta-analysis. Clinical Biochemistry, 137, 110911. https://doi.org/10.1016/j.clinbiochem.2025.110911

Vo-Dinh, T. (Ed.). (2014). Biomedical photonics handbook: biomedical diagnostics (Vol. 2). CRC press.

Walawender, L., Patterson, J., Strouse, R., Ketz, J., Saxena, V., Alexy, E., & Schwaderer, A. (2018). Mobile technology application for improved urine concentration measurement pilot study. Frontiers in Pediatrics, 6, 160.

Yeh, Y. L. (2008). Real-time measurement of glucose concentration and average refractive index using a laser interferometer. *Optics and Lasers in Engineering, 46*(9), 666-670.

Zentile, M. A., Offermans, P., Young, D., & Zhang, X. U. (2024). Fibre Refractometry for Minimally Invasive Sugar Content Measurements within Produce. *Sensors, 24*(19), 6336–6336. https://doi.org/10.3390/s24196336

Zirk, K., & Poetzschke, H. (2007). A refractometry-based glucose analysis of body fluids. *Medical engineering & physics, 29*(4), 449-458.